

Self-assembled growth of CeO₂ nanostructures on sapphire

J. C. Nie,* H. Yamasaki, and Y. Mawatari

*Energy Technology Research Institute, National Institute of Advanced Industrial Science and Technology (AIST),
1-1-1 Umezono, Tsukuba, Ibaraki 305-8568, Japan*

(Received 15 March 2004; revised manuscript received 3 August 2004; published 16 November 2004)

Experimental evidence of a self-assembly process was obtained where high-temperature O₂ annealing (1025 °C) induced a surface reorganization in CeO₂ deposited on *R*-cut sapphire substrates. Based on observation using atomic force microscopy and transmission electron microscopy, when the CeO₂ film was thin (<10 nm), a highly ordered phase was formed as large three-dimensional islands of CeO₂ with sapphire surface exposed. When the CeO₂ film thickness exceeded a critical value (~10 nm), an atomically-flat surface was formed by the reorganization. An energetics model based on these results was developed in which the formation energy of the island was calculated based on the observed facet configuration, taking into account the surface and interface energies, elastic strain, and short-range energy of edges. The energy minimization calculation showed that the calculated lateral and vertical dimensions agreed well with the observed shape of the islands. Based on the experimental evidence and these energy minimization calculations, we demonstrated that increasing the film thickness induces the important phase transition from large islands to an atomically-flat surface.

DOI: 10.1103/PhysRevB.70.195421

PACS number(s): 68.35.Bs, 61.46.+w, 68.55.Jk, 68.35.Md

I. INTRODUCTION

CeO₂ thin films have been extensively investigated because of their relatively high electrical conductivity,¹ chemical stability,² transmission in the visible and infrared regions,^{3,4} and efficiency for absorbing ultraviolet (UV) radiation.^{5,6} Besides, CeO₂ is a key component in the catalyst used for eliminating contaminants in automobile exhaust gases.^{7,8} It has also been proven that CeO₂ can act as an excellent buffer layer for high-*T_c* superconducting thin films.⁹ The fabrication and study of nanostructured CeO₂ thin films has been of interest due to new phenomena arising from the reduction in their dimensions. A phenomenon involving nanostructures is the quantum confinement effect.^{10,11} This effect, which has been well investigated for semiconductors, occurs when the crystal size approaches nanometer dimensions, and results in a shift in the absorption edge to higher energy, namely, increase in band gap energy. Lithographic techniques are now widely used to reduce lateral dimensions, the present resolution of far-UV lithography reaches ~100 nm. Nevertheless, quantum confined structures require lateral dimensions of 50 nm or less. Self-assembly, where ordered nanostructures are formed spontaneously on a crystal surface, is a low-cost, alternative method to produce nanostructures of very high structural quality.^{12,13}

In addition, the crystal growth on a lattice-mismatched substrate often proceeds via formation of 3D islands^{14–19} on a bare substrate surface for Volmer-Weber (VW) growth or on a wetted surface for *coherent* (dislocation-free) Stranski-Krastanov (SK) growth. Elastic strain can also cause spontaneous formation of 2D island domain structures,^{20–25} whose properties (such as domain size and topology) are well understood. Tersoff and Tromp theoretically showed that for 3D islands, a shape transition occurs as the islands increase in size.²⁶ Below a critical size, islands have a compact, symmetric shape, whereas above this size, they adopt a long thin

shape, which allows better elastic relaxation of the island's stress.

The growth mechanism of semiconductor thin films has been extensively investigated. However, studies on the growth of CeO₂ on sapphire substrate have been limited in number.^{5–7,9,13} Here, CeO₂ thin films were first grown on *R*-cut sapphire [Al₂O₃(1 $\bar{1}$ 02)] substrates and then annealed at high temperatures. The experimental methods enabled us to obtain experimental evidence of surface reorganization of CeO₂ film on a sapphire substrate. Then, we used atomic force microscopy (AFM) and transmission electron microscopy (TEM) to observe the morphology and the microstructure of the nanostructured thin films, revealing phase transition from large 3D islands to an atomically-flat surface when the film thickness was increased. Finally, based on these observations, we developed an energetics model for the island formation. This energetics model well explains the shape of the islands and the phase transition.

II. EXPERIMENT

The CeO₂ thin films were first grown on Al₂O₃(1 $\bar{1}$ 02) substrates by pulsed laser deposition utilizing a KrF excimer laser source (248 nm wavelength, Lambda Physik COMPex 205) operated at 300 mJ.^{13,27} The base pressure was on the order of 10⁻⁷ Torr and the oxygen pressure during the laser deposition was set at 300 mTorr. The distance between the target and substrate was about 55 mm. All CeO₂ films were prepared at a laser repetition rate of 1 Hz and a substrate temperature of 780 °C. After deposition the samples were annealed *in situ* in 400 Torr O₂ at 430 °C for 1 hour and then cooled to room temperature. The growth conditions described above are the typical conditions for oxide thin films.¹³ The resulting thin CeO₂ films, called as-grown samples, were further annealed *ex situ* at 1025 °C (Ref. 28)

in an O₂ flow for 1 hour and then cooled to room temperature.

Structural properties of the films were measured by using a thin film x-ray diffractometer (ATX-G, Rigaku Co.). ATX-G has additional goniometer axes so that it can conduct in-plane diffraction scans, as well as out-of-plane, or conventional $2\theta/\omega$ scans. In in-plane diffraction measurements, the sample and the detector rotate around the sample normal by ϕ and $2\theta_x$, respectively. The outgoing angle of the x ray to the surface is equal to the glancing angle ($\sim 0.3^\circ$), so that the diffraction plane is embedded in the surface plane. This is so-called the “in-plane diffraction.”^{29,30} X-ray diffraction (XRD) results showed that both the as-grown and high-temperature (1025 °C) annealed CeO₂ films were (001) textured with a high grade of in-plane orientation of CeO₂[100]||Al₂O₃[11 $\bar{2}$ 0] and CeO₂[010]||Al₂O₃[$\bar{1}$ 101], and that the crystalline quality of the film was improved by high-temperature O₂ annealing.¹³ Due to the high lattice perfection and smooth surfaces of the thin CeO₂ films, Laue oscillations appeared for both the as-grown and the annealed films. The nominal thickness t of the as-grown and the mean height h of the 3D islands of the annealed CeO₂ was then determined based on the adjacent satellite peaks from the Laue oscillations.³¹ In this study, the nominal thickness of the CeO₂ thin films ranged from 1.0 nm to 40.0 nm.

The morphology of the nanostructured surfaces of the films was then observed by AFM (Nanoscope III developed by Digital Instruments, Inc.). AFM images were recorded by using the tapping mode under an ambient atmosphere, at room temperature. The selected films were further observed in detail by TEM (Model JEM-2000EX) operated at 200 kV. Specimens for cross-sectional TEM were vertically cut along Al₂O₃[02 $\bar{2}$ 1] (i.e., [110] of CeO₂) and prepared by standard techniques including Ar ion milling.

III. RESULTS AND DISCUSSION

A. Observed microstructure of the nanostructured thin films

Figure 1 shows AFM images and corresponding cross-sectional profiles of four representative CeO₂ films (samples A, B, C, and D) of different thickness before and after the high-temperature O₂ annealing. The sapphire substrate surface was fully covered by the as-grown CeO₂ thin films for all the nominal thicknesses used in this study (>1.0 nm). The as-grown CeO₂ films showed small, round-shaped, and coalesced islands [Figs. 1(a), 1(c), 1(e), and 1(g)]. Line scan profiles showed that the root-mean-square (rms) surface roughness of the as-grown CeO₂ surfaces was about 0.55, 1.16, 1.52, and 1.65 nm for samples A, B, C, and D, respectively. After the high temperature (1025 °C) O₂ annealing, the surface of the thin CeO₂ films (<10 nm, e.g., 1.6-nm-thick sample A [Fig. 1(b)], 4.5-nm-thick sample B [Fig. 1(d)], and 8.4-nm-thick sample C [Fig. 1(f)]) showed a highly ordered phase. The phase was formed by 3D ordered islands of CeO₂ that were isolated or connected in groups. For sample A ($t=1.6$ nm), most of the 3D islands of CeO₂ were nearly isotropic (square) in shape and isolated with the dimensions of 11–23 nm wide and 15–27 nm long, and

10 ± 4 nm high [see Fig. 1(b)]. The islands were randomly distributed at the surface but were all oriented along the CeO₂[110]||Al₂O₃[02 $\bar{2}$ 1] and CeO₂[1 $\bar{1}$ 0]||Al₂O₃[20 $\bar{2}$ 1] in-plane directions. The cross-sectional profiles (from AFM images at smaller scales) drawn perpendicular to the edges of the islands, along the directions CeO₂[110] and CeO₂[1 $\bar{1}$ 0] revealed a well-defined angle with respect to the film plane: $\sim 54.74^\circ$ (see also the TEM data in the next paragraph). The edge facets determined from these cross sections correspond to crystallographic planes (111), ($\bar{1}\bar{1}$ 1), ($\bar{1}$ 11), and (1 $\bar{1}$ 1), respectively, and the top facet is (001). With increase in t (e.g., 4.5-nm-thick sample B), some of the isolated 3D islands started to be coalesced into large anisotropic (rectangular) islands, while most of the 3D islands of CeO₂ were still isolated with the dimensions of 40–100 nm wide, up to 400 nm long and 15 ± 5 nm high [see Fig. 1(d)]. With further increase in t (e.g., 8.4-nm-thick sample C), most of the isolated 3D islands were coalesced into large rectangular islands and were connected in groups. The dimensions of the large 3D islands of CeO₂ for sample C were 60–120 nm wide, up to 1000 nm long and 20 ± 5 nm high [see Fig. 1(f)]. The formation of the 3D ordered island phase did not occur for the CeO₂ films thicker than 10 nm. We therefore define “case I” as the formation of the large 3D ordered islands for the thin CeO₂ films with nominal thickness less than 10 nm, and define “case II” for the reorganization of the CeO₂ thin films with nominal thickness greater than 10 nm as below. When the CeO₂ thickness exceeded 10 nm (e.g., 12.4-nm-thick sample D), the self-assembly process induced by the O₂ annealing resulted in an atomically-flat surface that was clearly evident in the AFM images [Fig. 1(h)] as atomically-flat terraces and atomic steps. The rms surface roughness of the annealed CeO₂ surfaces was only about 0.15 nm for sample D.

Among the annealed CeO₂ films, we have chosen to evaluate the microstructure of sample B and sample D in detail because they were representative for case I and case II, respectively. The cross-sectional TEM images of large 3D islands (sample B) and an atomically-flat CeO₂ layer (sample D) are shown in Fig. 2. As can be seen clearly in Fig. 2(a), the islands formed in an isolated way and the sapphire surface was exposed due to the absence of any coverage outside the islands. TEM observations of the island formation also showed that the large 3D islands were coherent (dislocation-free). The strain contrast around the islands in Fig. 2(a) suggested that the local strain relaxation in the islands could result in elastic deformation of the substrate. This deformation lowers the energy of the island, at the cost of additional strain in the substrate. As demonstrated clearly in Fig. 2(a), the edge sides of the islands were beveled at a fixed angle of 54.74° to the sapphire substrate, indicating that the facets formed at the edge sides are corresponding to CeO₂(111), which has the lowest surface energy.^{32,33} From the other cross-sectional TEM images (data not shown), the observed dimensions of the islands were 40–400 nm long and about 11.5 ± 3.0 nm high. The observed height of the islands was well consistent with the XRD observation,³¹ while a little bit smaller than that by AFM. We prefer to believe the TEM and XRD data rather than the AFM data, since structures mea-

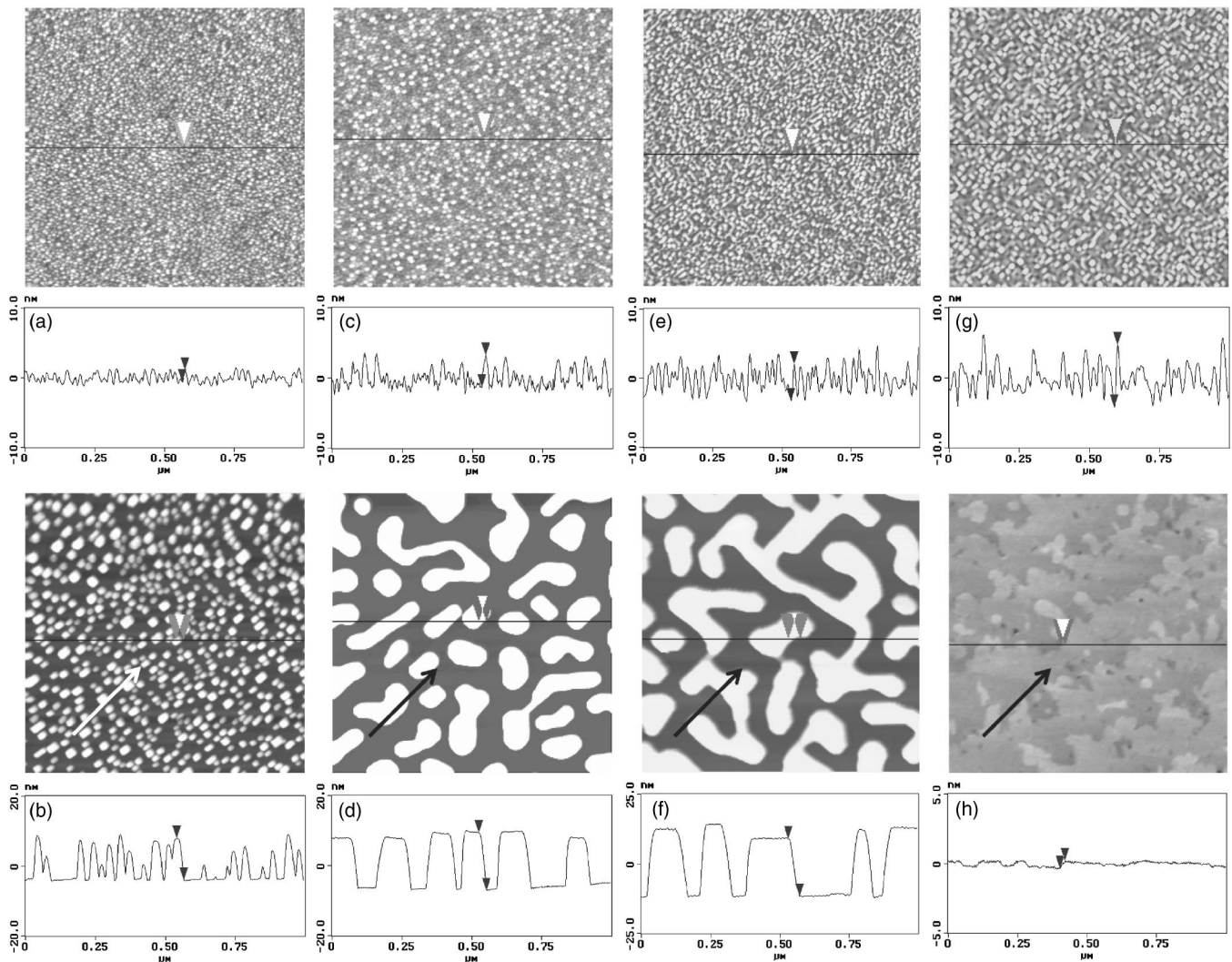


FIG. 1. AFM images and corresponding profiles of a 1.6-nm-thick CeO₂ film grown on *R*-cut sapphire (sample A) (a) before and (b) after high-temperature O₂ annealing at 1025 °C, a 4.5-nm-thick CeO₂ film (sample B) (c) before and (d) after the O₂ annealing, a 8.4-nm-thick CeO₂ film (sample C) (e) before and (f) after the O₂ annealing, and a 12.4-nm-thick CeO₂ film (sample D) (g) before and (h) after the O₂ annealing. The long arrows are parallel to the CeO₂ [110] direction.

sured by AFM could appear to be larger than what they are, due to the tip convolution effects. Also, the true heights of islands of samples A and C should be determined by XRD observation³¹ and were about 8.5 ± 2.5 and 16.0 ± 3.0 , respectively.

When the CeO₂ film exceeds 10 nm (e.g., 12.4-nm-thick sample D), a flat morphology was formed [Fig. 2(b)]. In addition, relief of the misfit strain in sample D could proceed by formation of misfit dislocations.³⁴ Figure 2(b) clearly shows that the dislocations originated at the CeO₂-Al₂O₃ interface and extended all the way up to the surface. Table I summarizes the measured lattice constants of the annealed CeO₂ thin films of various nominal thicknesses. The lattice distortion was defined as $e_i = (d_i - d_0) / d_0$, where d_i ($i = x, y, z$) is the measured hkl spacing and d_0 ($=0.54124$ nm) is the lattice parameter of cubic CeO₂ bulk. For samples A, B, and C (case I), the lateral misfit strain inside the CeO₂ films mainly relaxed by the formation of the 3D island phase. Besides, the lattice distortion in case I decreased with in-

crease of the nominal thickness of the CeO₂ films, i.e., the mean height of the 3D islands. The flat film (12.4-nm-thick sample D, case II) was found to contain less misfit strain (completely relaxed along Al₂O₃[$\bar{1}101$]) with smaller lattice distortion (see Table I). With further increase in t (e.g., 20.5-nm-thick sample E and 36.6-nm-thick sample F, case II), the lattice distortion varied slightly and the remained strain energy was accumulated inside the flat CeO₂ thin films. Considering the large lattice mismatch between CeO₂ and *R*-cut Al₂O₃ (3.7% along [$\bar{1}101$] and 12.1% along [$\bar{1}1\bar{2}0$] of sapphire, respectively, at room temperature), the small lattice distortion in case II ($<0.5\%$, see Table I) strongly suggests that the misfit strain between the film and substrate mostly relaxed by the introduction of dislocations.

High annealing temperature is necessary to provide enough thermal energy for the formation of the exposed sapphire surface and for the adatoms to assemble into 3D islands. The CeO₂ islands formed by the high temperature

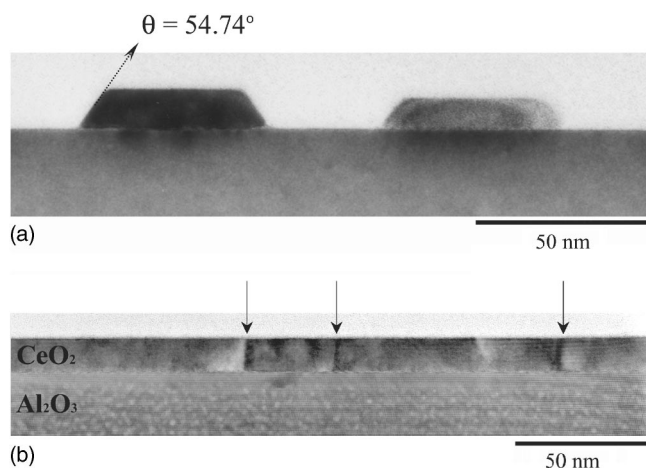


FIG. 2. Cross-sectional TEM images of (a) large 3D islands (4.5-nm-thick sample B) and (b) an atomically-flat CeO_2 layer (12.4-nm-thick sample D). Note that the strain contrast around the islands is clearly evident in (a), the bevel angle is 54.74° showing that the edge-side facet is CeO_2 (111); and the arrows in (b) indicate the representative dislocations.

(1025 °C) annealing on the $\text{Al}_2\text{O}_3(1\bar{1}02)$ surface displayed reproducible shapes, aspect ratios, and orientation [Figs. 1(b), 1(d), 1(f), and 2(a)].³⁵ With increase of the nominal thickness (t) of the CeO_2 thin films, the volume of each 3D island increases and the number density decreases. These results are analyzed quantitatively in Table II. For samples with small nominal thickness (e.g., 1.6-nm-thick sample A), islands displayed regular square or rectangular shapes and well-defined facets [see, e.g., Fig. 1(b)]. With increase in t (but < 10 nm, e.g., 4.5-nm-thick sample B and 8.4-nm-thick sample C), most of islands presented more complex and irregular shapes, which can be found from the AFM images [see, e.g., Figs. 1(d) and 1(f)]. Indeed, these islands are the

result of the coalescence of several smaller islands. The probability to observe this type of islands as well as the total coverage of the exposed sapphire surface increased with increase of the nominal thickness of the CeO_2 films.

Such 3D islands underwent a phase transition when the film thickness was increased. Below a critical thickness of 10 nm, islands were 3D and adopted an elongated shape, which allows better elastic relaxation of the island's stress. Above this critical thickness, a uniform phase of an atomically-flat thin layer was formed. As the island growth proceeded close to equilibrium due to the high temperature annealing, the morphology of the islands should be governed by the minimization of its total energy. To explain the phase transition and the shape of the islands obtained after the high temperature annealing, we developed an energetics model described in the next section.

B. Description of the energetics model

From AFM and TEM observations (Fig. 1 and Fig. 2), the typical shape of the self-assembled islands obtained by the high temperature O_2 annealing can be modeled. For simplicity, in the model we assumed the island to be rectangular in shape, with half-width a (width at the half maximum height), half-length b , and height h , in the x , y , and z directions, respectively [see Figs. 3(a) and 3(b)]. The edge sides were beveled at an angle of θ to the substrate [see Figs. 3(c) and 3(d)]. Figures 3(c) and 3(d) show schematics of the assumed surface reorganization for cases I and II, respectively. Although the actual surface of the as-grown CeO_2 films was not uniformly flat (actually it showed a rough coverage with a rms surface roughness up to 1.65 nm; see Fig. 1), for simplicity, the CeO_2 thin film before the reorganization was assumed to have a flat surface, as illustrated by the dashed rectangles in Figs. 3(c) and 3(d). For case I, the reorganized CeO_2 surface was assumed discontinuous and the substrate

TABLE I. Lattice constant d_i (the pseudomorphic azimuths of $\text{CeO}_2[100]$, $[010]$ and $[001]$ were defined as parallel to $\text{Al}_2\text{O}_3[11\bar{2}0]$, $[\bar{1}101]$ and $[1\bar{1}02]$, respectively; note that the lattice constants of R -cut sapphire substrate are 0.476 nm, 0.521 nm, and 0.347 nm along $[11\bar{2}0]$, $[\bar{1}101]$, and $[1\bar{1}02]$, respectively) of the annealed CeO_2 films of various nominal thickness t , and calculated lattice distortion e_i . [Lattice distortion defined as $e_i = (d_i - d_0)/d_0$, where d_i ($i=x,y,z$) is the measured hkl spacing and d_0 ($=0.54124$ nm) is the lattice parameter of cubic CeO_2 bulk.] The six representative samples are classified by the two different phases, case I and case II, respectively. All films were deposited by PLD using the same deposition parameters (laser energy of 300 mJ, laser repetition rate of 1 Hz, substrate temperature of 780 °C, and O_2 pressure of 300 mTorr) and *ex situ* annealed at 1025 °C in an O_2 flow for 1 h and cooled to room temperature.

Sample	t (nm)	Phase	d_x/e_x (nm/%)	d_y/e_y (nm/%)	d_z/e_z (nm/%)
A	1.6	I	0.53787/-0.62	0.53730/-0.73	0.54062/-0.11
B	4.5		0.53979/-0.27	0.53803/-0.59	0.54029/-0.18
C	8.4		0.54019/-0.19	0.53906/-0.40	0.54047/-0.14
D	12.4	II	0.53931/-0.36	0.54140/0.03	0.53943/-0.33
E	20.5		0.53963/-0.30	0.53987/-0.25	0.53923/-0.37
F	36.6		0.53912/-0.39	0.53871/-0.47	0.53927/-0.36

TABLE II. Average characteristics of the islands obtained by the high-temperature O₂ annealing, for the nominal thickness $t=1.6$ nm, 4.5 nm, and 8.4 nm. The mean lateral dimensions \bar{a} and \bar{b} were determined through a statistical analysis of about 50 islands of the AFM images. The mean height \bar{h} was determined by the XRD and TEM observations. The standard deviation (except few very elongated islands) is given in brackets. The number density d of the islands is determined by counting the number of the isolated 3D islands per μm^2 . Islands, which have the complex and irregular shapes and are totally connected, are regarded as one island for the number density estimation.

Sample	t (nm)	\bar{a} (nm)	\bar{b} (nm)	\bar{h} (nm)	d (/ μm^2)	Coverage (%)	Aspect ratios	
							\bar{b}/\bar{a}	\bar{h}/\bar{a}
A	1.6	16.5(5)	19.5(5)	8.5(2.5)	720	25	1.20(0.20)	0.49(0.12)
B	4.5	70(30)	160(120)	11.5(3.0)	40	35	2.46(1.46)	0.18(0.05)
C	8.4	90(30)	320(200)	16.0(3.0)	20	48	3.76(2.76)	0.18(0.05)

surface as bare Al₂O₃(1 $\bar{1}$ 02) [Fig. 3(c)]. For case II, the formation of the islands (if any) was assumed to occur on top of the CeO₂ layer (partially relaxed by the dislocations) and the appropriate reference was not the bare sapphire surface but CeO₂(001) [Fig. 3(d)]. Accordingly, in our model, we do not consider more general possible shape for the CeO₂ island, but only (001) and (111) facets ($\theta=54.74^\circ$). Although in general an actual island might have a more complex shape than these facets, including edge rounding at high temperatures, the shape assumed here is sufficient to capture the important features such as size and aspect ratios.

We take the sapphire substrate as our energy reference, plus a reservoir of CeO₂ strained to match sapphire in the x and y directions, and free to relax in the z direction. Then the energy change of the formation of an isolated island due to the surface reorganization can then be written as

$$E = E_s + E_e + E_{el}, \quad (1)$$

where E_s is the extra surface and interface energy, E_e is the short-range energy of edges,³⁶ and E_{el} is the energy change due to elastic relaxation.

First we consider the elastic relaxation energy, the third term in Eq. (1), E_{el} . Due to the lattice mismatch between CeO₂ and R -cut Al₂O₃ (3.7% along $[\bar{1}101]$ and 12.1% along $[11\bar{2}0]$ of sapphire, respectively, at room temperature; and 4.1% and 12.4%, respectively, at 1025 °C), epitaxial layers of CeO₂ on sapphire are highly strained. Prior to relaxation, the 2D stresses at the surface generate a force, which elastically distorts the substrate. This distortion lowers the energy of the island, at the cost of additional strain in the substrate [see, e.g., Fig. 2(a)].^{26,37} Actually, the lattice mismatch between the island and the substrate introduces an elastic-force monopole f [see, e.g., the illustration in Fig. 3(a)] along the island periphery^{21,24,25} proportional to the misfit strains. Earlier studies of strained islands relied on numerical finite-element calculations, taking the height effect into account.^{38,39} An explicit approximation for the elastic relaxation energy was derived by Tersoff and Tromp,²⁶ yielding good understanding of island behavior. Based on their derivation²⁶ and considering an anisotropic solid, the elastic relaxation energy of island formation can be written as

$$E_{el} = -\Lambda h^2 \left[b \ln \left(\frac{a}{\phi h} \right) + a \ln \left(\frac{b}{\phi h} \right) \right], \quad (2)$$

where $\Lambda = f^2(1-\nu)/\pi\mu$, μ is the shear modulus, ν is Poisson's ratio, and $\phi = e^{-3/2} \cot \theta$ is the parameter related to the microscopic cutoff length and the geometry of the island edges. For case I (heteroepitaxial), $f = (\sigma_a + \sigma_b)/2$ represents the elastic force monopole along the island periphery induced by the lattice mismatch between the island and substrate [see Fig. 3(a)].²⁴ For case II (homoepitaxial), $f = (\sigma_a - \sigma_b)/2$ represents the elastic force monopole induced by the surface stress anisotropy [see Fig. 3(b)].^{21,25} Here, σ_a and σ_b are the xx and yy components of the 2D island stress tensor of CeO₂ biaxially strained in an anisotropic way to the Al₂O₃ x and y lattice constants. We neglect the variation of σ as the island relaxes in the z direction, i.e., the variation of σ as the function of the island height h , a higher-order effect.

The short-range energy of island edges, E_e , which is always positive, was not taken into account in the study by Tersoff and Tromp.²⁶ However, Shchukin^{36,37} and Marchenko⁴⁰ showed that for a lattice-mismatched system with edge-side facets, both E_e and E_{el} should be taken into account. Marchenko⁴⁰ showed that E_e , the short-range contribution from the island edges, can be incorporated into the total relaxation energy E_{el} by introducing a renormalized ϕ . The terms $E_e + E_{el}$ can then be represented by the following particularly simple form when E_e is expressed in terms of β and β is incorporated inside Θ :

$$E_e + E_{el} = -\Lambda h^2 \left[b \ln \left(\frac{a}{\Theta h} \right) + a \ln \left(\frac{b}{\Theta h} \right) \right], \quad (3)$$

where $\Theta = e^{\beta-3/2} \cot \theta$. The parameter β can be fitted by the numerical simulations. The best overall fit to our experimental data was with $\beta=3.3$ (see next paragraph).

Equation (3) is an excellent approximation for $E_e + E_{el}$ if $a \gg h$ and $b \gg h$, and can be rearranged into a generic compact form:

$$E_e + E_{el} = \Lambda D h^2 \left[\left(c - \frac{1}{c} \right) \ln c - \left(c + \frac{1}{c} \right) \ln \frac{D}{\Theta h} \right], \quad (4)$$

where $D = \sqrt{ab}$ is the effective diameter of the island, and $c^2 = b/a$ is the lateral aspect ratio of the island. The first term

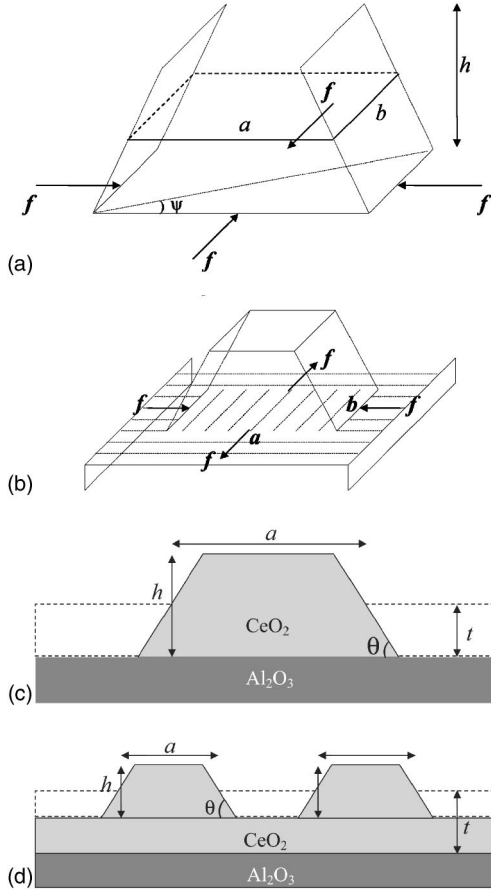


FIG. 3. Schematic views of the assumed shape of 3D islands grown on sapphire substrate. $\psi = \arctan(b/a)$ defines the aspect ratio of the island. (a) Case I (heteroepitaxial). $f = (\sigma_a + \sigma_b)/2$ represents the elastic force monopole along the island periphery induced by the lattice mismatch between the island and substrate. (b) Case II (homoepitaxial). Dashed lines indicate alternating stress domains arising from surface stress anisotropy. $f = (\sigma_a - \sigma_b)/2$ represents the elastic force monopole induced by the surface stress anisotropy. Note that the force monopole on the two a sides points in a direction opposite to the force monopole in case I, shown in (a). 2D views of (c) formation of coherent 3D islands on bare sapphire substrate (case I) and (d) formation of 3D islands on top of the atomically-flat CeO_2 layer (case II), showing cross section in xz plane, and illustrating the definition of half-width a , height h , and contact angle θ . The dashed rectangles represent the as-grown CeO_2 volumes before the surface reorganization.

is positive (note that this term vanishes for a square island of $c=1$), and the second term is always negative.

C. Formation of the 3D islands (case I)

Based on our energetics model, the formation of coherent 3D islands (case I) on the bare sapphire substrate is due to the surface reorganization of the as-grown CeO_2 film via the high-temperature O_2 annealing [see Fig. 3(c)]. The nominal thickness t of the as-grown CeO_2 film is a given constant. Omitting the h^2 terms corresponding to the corners, the extra surface and interface energy of the island formation can be written as

TABLE III. Surface energies of CeO_2 surfaces. (Data of the unrelaxed and relaxed surface energies of CeO_2 are from Refs. 32 and 33.)

Surface	Energy (J/m^2)	
	Unrelaxed	Relaxed
(111)	1.737	1.537
(110)	3.590	2.451
(100)	6.453	3.251
(211)	7.638	2.674

$$E_s = \gamma_1 \left(\frac{h}{t} - 1 \right) ab - \Gamma_1 (a + b)h, \quad (5)$$

where $\gamma_1 = u_s - u_i - u_t$ and $\Gamma_1 = u_i \cot \theta + u_s \cot \theta - u_i \cot \theta - 2u_e \csc \theta$. Before the island formation, t ($\leq h$) is the nominal thickness of the CeO_2 slab [illustrated by the dashed lines in Fig. 3(c)], which has the same volume as the island. Here, u_s , u_t , and u_e , are the surface energy (per unit area) of the substrate and of the island's top and edge-side facets, respectively, and u_i is the island-substrate interface energy. Considering that the as-grown CeO_2 thin films were pseudomorphic as determined by XRD (Ref. 13) and the fact that the formation of the exposed sapphire surface requires sufficient high annealing temperature, CeO_2 is thought to be able to easily wet the sapphire surface. The interface energy u_i is therefore not expected to play a major role with respect to the surface energies ($> 1.5 \text{ J}/\text{m}^2$), although it is expected to be positive. In the model, we assumed that the surface energies and the contact angles for both the edge-side facets a and b are equivalent. Equation (5) is an excellent approximation if the strained CeO_2 is pseudocubic. The first term is the change in E_s for flat surfaces. The second term is the "creation energy" of the island edge sides.

In our model, we used the surface energies per unit area computed in Refs. 32 and 33, as shown in Table III. The four lowest surface energies for CeO_2 are (111), (110), (100), and (211). In case I, contribution from the exposed $\text{Al}_2\text{O}_3(1\bar{1}02)$ should also be considered. The fracture surface energy of the sapphire R -plane is $U_{(1\bar{1}02)} = 6.0 \text{ J}/\text{m}^2$.⁴¹ Taking the relaxed data from Table III for the different surfaces of CeO_2 and assuming that the island-substrate interface energy u_i plays an insignificant role, then $\gamma_1 > 0$ and $\Gamma_1 > 0$. For CeO_2 materials, the creation energy of the island edge sides [the second term in Eq. (5)] is *negative* when the edge-side facet is considered (111) and the top facet is considered (001).

For a *dilute* system of islands of sparse distribution, the elastic interaction between islands via the strained substrate might be insignificant. Then, combining Eqs. (4) and (5), the formation energy E of the island can be written as

$$E = \gamma_1 \left(\frac{h}{t} - 1 \right) D^2 - \Gamma_1 \left(c + \frac{1}{c} \right) Dh + \Lambda D h^2 \left[\left(c - \frac{1}{c} \right) \ln c - \left(c + \frac{1}{c} \right) \ln \frac{D}{\Theta h} \right]. \quad (6)$$

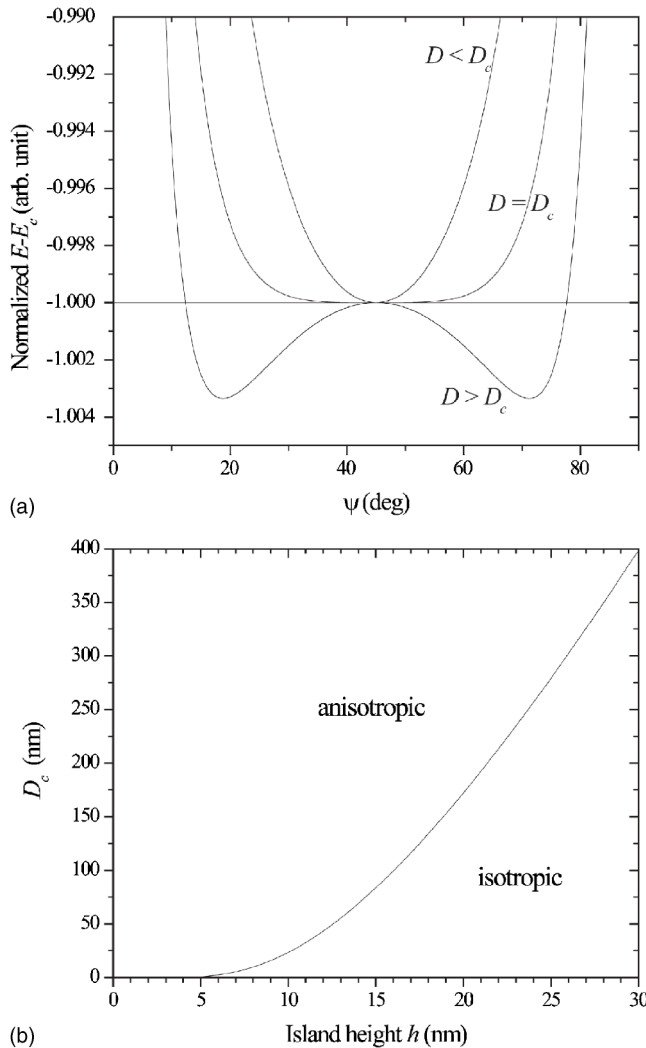


FIG. 4. (a) Formation energy, relative to E_c , of an isolated island as a function of angle $\psi = \arctan(b/a)$ for different island sizes D , demonstrating the strain-induced shape instability. Islands with $D < D_c$ adopt an isotropic (square) shape, while those with $D > D_c$ adopt an elongated anisotropic (rectangular) shape. (b) The calculated critical size $D_c [= e^2 \Theta h \exp(-\Gamma_1/\Lambda h)]$ as a function of h . For the calculation, $\beta = 3.3$ and $\Lambda = \Gamma_1/26 \text{ nm}^{-1}$.

First we consider the shape instability. Figure 4 illustrates the strain-induced shape instability. The parameter for the lateral aspect ratio of an island is defined as $\psi = \arctan(b/a)$ [see Fig. 3(a)]. In our model, we selected ψ instead of the aspect ratio b/a as the parameter for island shape, because the total energy of the island E is symmetric about $\psi = 45^\circ$. A small island ($D < D_c$) always adopts a isotropic (square) shape. As the island size exceeds a critical size D_c , the isotropic shape becomes unstable and strain induces a spontaneous shape instability: the island adopts a rectangular shape elongated in either of the two orthogonal directions with two degenerate energy minima at $\psi_m = 45^\circ \pm \Delta\psi$. $\Delta\psi$, and hence the lateral b/a of the elongated islands, increases with increasing island diameter (D). The critical size D_c is defined by the condition

$$\left. \frac{d^2 E}{d\psi^2} \right|_{\psi=45^\circ} = 0,$$

thus yielding

$$D_c = e^2 \Theta h \exp\left(-\frac{\Gamma_1}{\Lambda h}\right). \quad (7)$$

For a given size $D = \alpha D_c$, E can be written as

$$E = E_c + \Lambda D h^2 \left[\left(c - \frac{1}{c}\right) \ln c - \left(c + \frac{1}{c}\right) (2 + \ln \alpha) \right]. \quad (8)$$

The first term, $E_c = D^2(h/t-1)\gamma_1$, is independent of ψ . In Fig. 4(a), the calculated formation energy $E - E_c$ of an island is shown as a function of ψ for different island sizes (different D). In Fig. 4(b), the calculated critical size D_c is shown as a function of h . These calculations illustrate the strain-induced shape instability and were clearly verified by experimental observation [Figs. 1(b), 1(d), and 1(f)]. The existence of the spontaneous shape instability originates from the competition between the strain relaxation energy Λ and the surface energy Γ_1 .²⁴ It is especially obvious in the limit conditions. When $\Gamma_1/\Lambda h \ll 1$, i.e., the island stress dominates, the strain relaxation energy shifts the critical size D_c to a larger value, and thus drives the island toward an isotropic (square) shape. If the surface energy dominates ($\Gamma_1/\Lambda h \gg 1$), the isotropic surface energy shifts the critical size D_c to a smaller value and drives the island toward an anisotropic (rectangular) shape. Although in this study Γ_1 is considered equivalent for both the edge-side facets a and b , such a strain-induced shape instability has been demonstrated theoretically by Li *et al.*²⁴ for the strained islands with either the isotropic or anisotropic surface (facet) energies.

Next we consider the equilibrium height of the islands. We limit our discussion to the reorganization of a static film (no deposition) at the thermodynamic limit. The spontaneous formation of large 3D islands occurs randomly. The islands might contain CeO₂ materials of different volumes with various dimensions. In Fig. 5, the calculated $E(h) + \gamma_1 D^2$ is shown as a function of h with (a) $c=1$ and $t=4.5 \text{ nm}$ and (b) $c=2$ and $t=8.4 \text{ nm}$ for various D . The calculation shows that if D exceeds a threshold value [$D_m \sim 101 \text{ nm}$ for (a) $c=1$ and $t=4.5 \text{ nm}$, $D_m \sim 302.5 \text{ nm}$ for (b) $c=2$ and $t=8.4 \text{ nm}$], the energy increases monotonically with h , and the formation of the island will not occur. For $D < D_m$, however, $E(h)$ has a well-defined minimum at h_e , the equilibrium height of the island at which $dE/dh=0$. At small D [$< 60 \text{ nm}$ for (a) $c=1$ and $t=4.5 \text{ nm}$, $< 210 \text{ nm}$ for (b) $c=2$ and $t=8.4 \text{ nm}$], h_e increases with increasing D , whereas at larger D , h_e decreases with increasing D . The estimated h_e is up to 11.0 nm for (a) $c=1$ and $t=4.5 \text{ nm}$ and up to 16.2 nm for (b) $c=2$ and $t=8.4 \text{ nm}$, respectively, which is fairly consistent with experimental observations [see, e.g., Fig. 2(a) and Table II].

Next we consider the size selection of the islands. In Fig. 6, calculated $E(D)$ is shown as a function of D with $c=2.5$, $h=10 \text{ nm}$ (a), 15 nm (b), and 20 nm (c) for various t . The t was selected to start from 1.24 nm in Fig. 6(a) [2.7 nm in Fig. 6(b) and 4.05 nm in Fig. 6(c)], because for $t < 1.24 \text{ nm}$

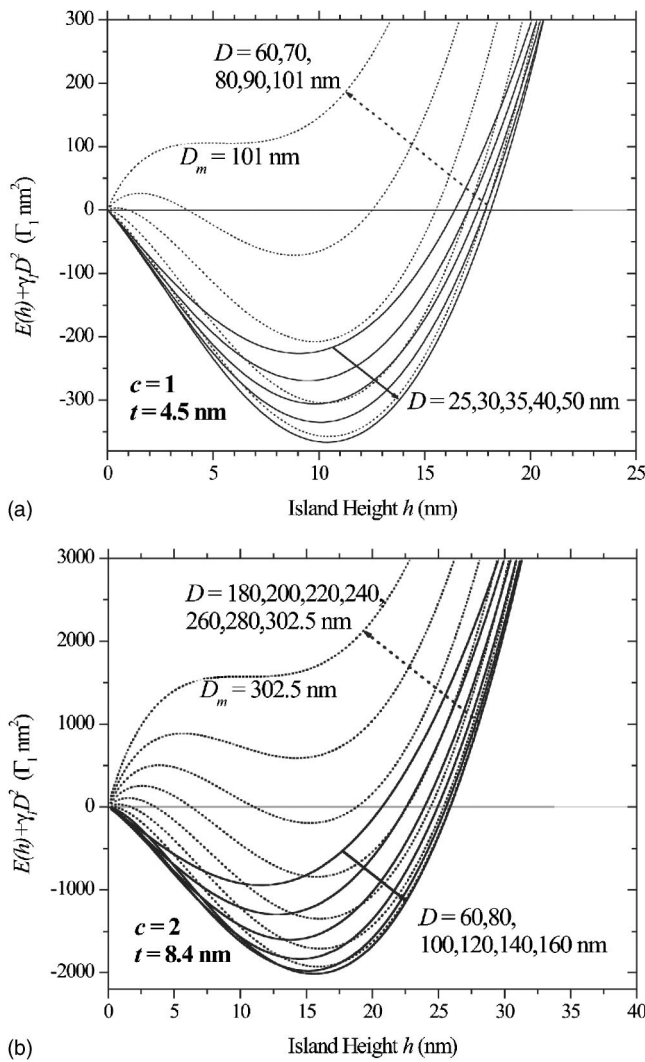


FIG. 5. Formation energy, relative to $-\gamma_1 D^2$, of an isolated island as a function of height h for several island sizes D . The lateral aspect ratio of the island and the nominal thickness of the as-grown CeO_2 film were assumed to be (a) $c=1$ and $t=4.5$ nm and (b) $c=2$ and $t=8.4$ nm, respectively. For the fitting, $\beta=3.3$, $\gamma_1=\Gamma_1/8$, and $\Lambda=\Gamma_1/26 \text{ nm}^{-1}$.

(2.7 nm/4.05 nm), $E(D)$ increases monotonically with size, and the formation of the island will not occur. The calculation shows that at very small D (<2 nm for $h=10$ nm, <8 nm for $h=15$ nm, and <17 nm for $h=20$ nm), $E(D)$ increases with increasing D . The island can be stable above a critical nucleus size, D_n , at which $dE/dD=0$, and an increase in D is accompanied by a decrease in E . At large D , E again increases due to the D^2 -dependence of the surface energy term. At intermediate D , E has a well-defined minimum at a stable island size D_s , at which $dE/dD=0$. The stable island size D_s can be proportionally controlled by varying t . As t is increased, D_s increases, diverging as t approaches h [i.e., the first term (D^2 term) in Eq. (6) vanishes]. The curves in Fig. 6 show that stable islands are not necessarily energetically favorable. If $t < \sim 1.58$ nm (3.44 nm/5.12 nm), E is still positive, and the islands are metastable and thus may adopt an anisotropic shape [or even an isotropic shape ($c=1$)] with

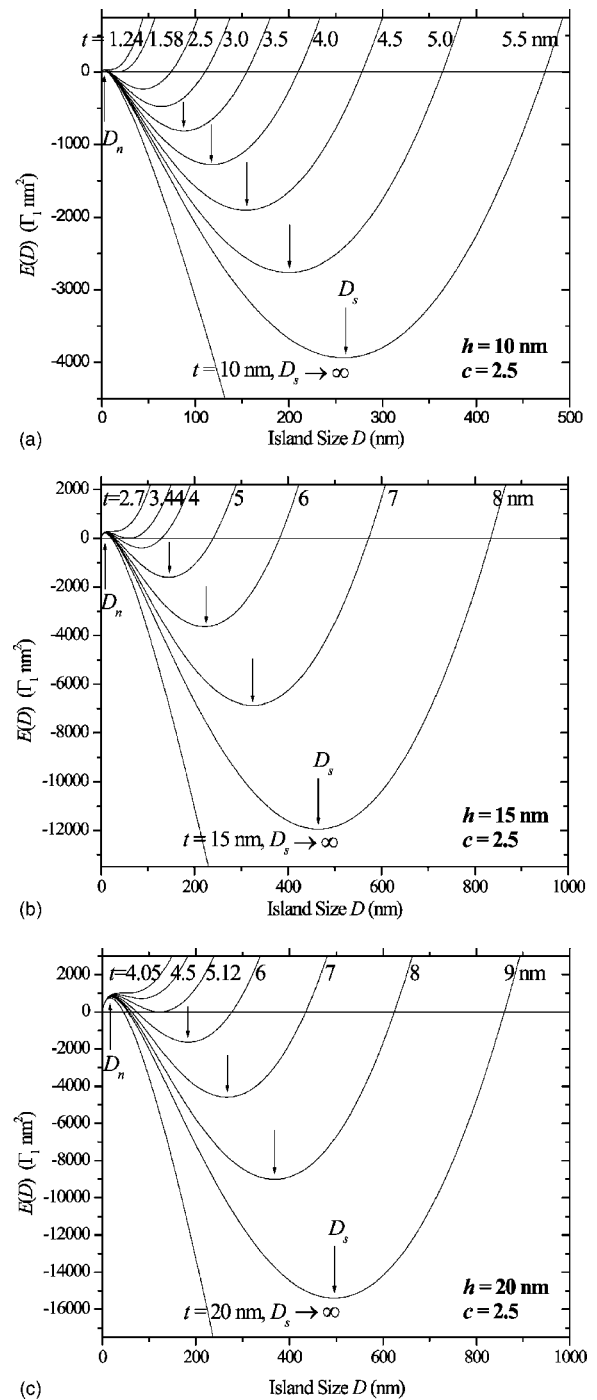


FIG. 6. Formation energy, E , of an isolated island as a function of island size D for several thicknesses t . The lateral aspect ratio of the island was assumed to be $c=2.5$. Island height h was fixed at 10 nm (a), 15 nm (b) and 20 nm (c), respectively. For the fitting, $\beta=3.3$, $\gamma_1=\Gamma_1/8$ and $\Lambda=\Gamma_1/26 \text{ nm}^{-1}$.

height less than 10 nm (15 nm/20 nm). This was confirmed by our experimental results [see, e.g., Figs. 1(b), 1(d), and 1(f) and Table II]. Because spontaneously formed islands might contain different volumes of CeO_2 , as discussed in the preceding paragraph, islands with volume $V < D_s^2 h$ could not reach D_s described in Fig. 6 but could reach a minimum E with size less than D_s , whereas islands with $V > D_c^2 h$ might

adopt an anisotropic shape with $c > 2.5$ due to the shape instability. Despite all this, the relation between D_s and t is qualitatively consistent with AFM observation [Figs. 1(b), 1(d), and 1(f) and Table II].

Two effects on island growth involve t_c (the critical value of t , above which no island forms). First, when D exceeds a critical size D_c , the island becomes anisotropic. For an isotropic island, the last term in Eq. (6) dominates, and the energy minimization requires maximizing c , thus favoring a large D_s . Second, groups of islands are not necessarily isolated from each other. Not only isolated isotropic islands, but also groups of anisotropic islands near equilibrium have various D , as shown in Figs. 1(d) and 1(f). With increase in t , the islands become closer to each other and the island-island interaction (via the strained substrate) becomes significant. Because the interaction between islands is repulsive,^{36,42} the configuration with isolated islands has a higher energy than the uniform phase (flat surface without formation of 3D islands), which makes the 3D island phase unstable. On the other hand, the competition between strain energy buildup and strain relief due to dislocation nucleation also leads to a concept of the equilibrium critical thickness, at which the energy of the strained epitaxial state is equal to that of a state containing a single misfit dislocation.³⁴ Due to the shape instability, the repulsive island-island interaction and the introduction of dislocations, t_c is about 10 nm (according to the experimental data), less than the analytical value, which is the equilibrium height h_e (e.g., 16.0 ± 3.0 nm when $t = 8.4$ nm). When $t > t_c$, a phase transition from the 3D ordered islands (case I) to an atomically-flat thin layer (case II) takes place. In the following, we present the argument that the atomically-flat surface is energetically favorable for case II.

D. Formation of the atomically-flat surface (case II)

Based on our energetics model, the island formation of case II (if any) is due to the surface reorganization in the top layer of the as-grown CeO₂ film [see the schematic drawing in Fig. 3(d)]. In case II, the sapphire substrate is not exposed any more and we just take the sapphire substrate plus the partially relaxed CeO₂ base layer (by the introduction of dislocations) as the energy reference. In this case, $u_t = u_s$ and $u_i = 0$, and thus $\gamma_2 = 0$ and $\Gamma_2 = 2(u_t \cot \theta - u_e \csc \theta)$. Taking the relaxed data from Table III for the different surfaces into the expression of Γ_2 , then $\Gamma_2 > 0$. Thus, E_s for case II can be written as

$$E_s = -\Gamma_2(a+b)h. \quad (9)$$

In case II, we do not fix the total volume ($V = D^2h$) of the island in the model, but instead consider E/V , which can be written as

$$\frac{E}{V} = -\Gamma_2 \left(c + \frac{1}{c} \right) \frac{1}{D} + \Lambda \frac{h}{D} \left[\left(c - \frac{1}{c} \right) \ln c - \left(c + \frac{1}{c} \right) \ln \frac{D}{\Theta h} \right]. \quad (10)$$

Following the method by Tersoff and Tromp,²⁶ we consider the equilibrium shape by minimizing the energy with

respect to c and D , keeping h fixed. The minimization of E/V with respect to c and D leads to $c = 1$ and $D = D_0$, where

$$D_0 = e\Theta h \exp\left(-\frac{\Gamma_2}{\Lambda h}\right). \quad (11)$$

With decreasing h , the equilibrium island size D_0 decreases much faster (exponentially) than h (linearly). In other words, even if h varies, the change in h is slow compared with the change in lateral dimension D . Thus, the validity of Eq. (11) is self-consistent with the assumption of fixed h . As shown in Eq. (11), the minimal-energy island size is $D_0 = e\Theta h e^{-\Gamma_2/\Lambda h}$. At this D_0 ,

$$\left. \frac{\partial E/V}{\partial h} \right|_{D=D_0} = \frac{2\Gamma_2}{Dh} > 0. \quad (12)$$

The energy minimization requires minimizing h ! Thus, at the thermodynamic limit, the islands should always “shrink” until each island vanishes, resulting in an atomically-flat surface.

In fact, all the values for the surface (facet) energies drastically depend on the accumulated strain energy in a way which is rather difficult to predict. The surface energy of the island’s top, u_t , and the surface energy of the island’s edge facet, u_e , and therefore Γ_2 are actually t - and h -dependent, i.e., $\Gamma_2(t, h) = 2[u_e(t, h)\csc\theta - u_t(t, h)\cot\theta]$. Considering this h -dependence of Γ_2 (even Λ) and the assumption of the constant h in deriving the equilibrium island size D_0 , the expression of the partial differential $\partial(E/V)/\partial h$ [see Eq. (12)] is not very accurate. Nevertheless, the qualitative conclusion drawn from Eq. (12), i.e., the formation of the atomically-flat surface, is well consistent with the experimental observations [see, e.g., Fig. 1(h) and Fig. 2(b)].

The key conclusions for both case I and case II depend significantly on the sign of γ_1 , Γ_1 and Γ_2 , which is quite unique for CeO₂. For example, in CeO₂ material, the creation energy of the island edge sides [the second term in Eq. (6) and the first term in Eq. (10)] is negative when the edge-side facet is (111) and the top facet is (001). Despite such dependence, the analytical expression for the short-range and relaxation energy, such as Eq. (3), can help identify fundamental regimes of behavior for strained-layer reorganizations. Although several approximations were made in deriving Eq. (3), including the neglect of the “corner” terms and the variation of stress tensor σ as the island relaxes in the z direction, which requires $D \gg h$,²⁶ and the incorporation of E_e into E_{el} by renormalizing Θ analogous to Marchinko,⁴⁰ the result gives an accurate picture of surface reorganization of strained CeO₂ islands on sapphire via the high-temperature O₂ annealing. Thus, the key conclusions here do not depend on the approximations underlying Eq. (3). An exact calculation, if possible, would only shift the equilibrium dimensions (D_s, h_e in case I) of the islands and the critical thickness t_c at which the phase transition occurs.

IV. SUMMARY

Epitaxial CeO₂ thin films were fabricated by pulsed laser deposition on R -cut sapphire substrates. Experimental evi-

dence of a self-assembly process was obtained where high-temperature O_2 annealing (1025 °C) induced a surface reorganization in the as-grown CeO_2 films. When the CeO_2 film exceeded a critical thickness (~ 10 nm), an atomically-flat surface was preferred. When the CeO_2 film was thin (< 10 nm), the formation of large 3D ordered islands of CeO_2 proceeded, leaving most of the substrate surface exposed. The self-assembled CeO_2 islands were found to be faceted by perfect crystallographic planes of (111) and (001). Therefore, under these conditions, the self-assembly process is thought to proceed close to equilibrium. An energetics model was proposed based on these observed facet configurations. The formation energy of an island was calculated, taking into account surface and interface energies, elastic strain, and short-range energy of edges. The energy minimi-

zation calculation showed that the calculated lateral and vertical dimensions of an island are well consistent with the equilibrium shape of the islands observed by AFM and TEM. In conclusion, increasing the film thickness induces the important phase transition from large islands to an atomically-flat surface.

ACKNOWLEDGMENTS

J.C.N. is grateful to Professor Tromp (IBM, USA) for stimulating discussion of the manuscript. This work has been carried out as a part of the Super-ACE Project (R&D of Fundamental Technologies for Superconducting AC Power Equipment) of the Ministry of Economy, Trade and Industry (METI).

*Corresponding author. Present address: Department of Physics, Beijing Normal University, Beijing 100875, China. Email address: jcnie@bnu.edu.cn

- ¹C. R. A. Catlow, *Solid State Ionics* **12**, 67 (1984).
- ²O. T. Sørensen, *J. Solid State Chem.* **18**, 217 (1976).
- ³R. M. Bueno, J. M. Martinez-Duart, M. Hernandez-Velez, and L. Vazquez, *J. Mater. Sci.* **32**, 1861 (1997).
- ⁴A. Hartridge, M. G. Krishna, and K. Bhattacharya, *J. Phys. Chem. Solids* **59**, 859 (1998).
- ⁵S. Guo, H. Arwin, S. N. Jacobsen, K. Järrendahl, and U. Helmerson, *J. Appl. Phys.* **77**, 5369 (1995).
- ⁶T. Suzuki, I. Kosacki, V. Petrovsky, and H. U. Anderson, *J. Appl. Phys.* **91**, 2308 (2002).
- ⁷B. Harrison, A. F. Diwell, and C. Hallett, *Platinum Met. Rev.* **32**, 73 (1988).
- ⁸See several papers in *Catalysis and Automotive Pollution Control II*, edited by A. Crucq, Studies in Surface Science and Catalysis, Vol. 71 (Elsevier, Amsterdam, 1991); C. Morterra, V. Bolis, and G. Magnacca, *J. Chem. Soc., Faraday Trans.* **92**, 1991 (1996); S. Tagliaferri, R. A. Koppel, and A. Baiker, *Appl. Catal.*, **B** **15**, 159 (1998); J. M. A. Harmsen, J. H. B. J. Hoebink, and J. C. Schouten, *Chem. Eng. Sci.* **56**, 2019 (2001).
- ⁹X. D. Wu, R. C. Dye, R. E. Muenchausen, S. R. Foltyn, M. Maley, A. D. Rollett, A. R. Garcia, and N. S. Nogar, *Appl. Phys. Lett.* **58**, 2165 (1991).
- ¹⁰M. I. Freedhoff and A. P. Marchetti, *Optical Properties* (CRC, New York, 1997), Vol. 2, pp. 1–30.
- ¹¹L. E. Brus, *J. Chem. Phys.* **80**, 4403 (1984).
- ¹²H. Brune, M. Giovannini, K. Bromann, and K. Kern, *Nature (London)* **394**, 451 (1998).
- ¹³J. C. Nie, H. Yamasaki, H. Yamada, Y. Nakagawa, and K. D. Develos, *Supercond. Sci. Technol.* **16**, 768 (2003).
- ¹⁴D. J. Eaglesham and M. Cerullo, *Phys. Rev. Lett.* **64**, 1943 (1990).
- ¹⁵Y. W. Mo, D. E. Savage, B. S. Swartzentruber, and M. G. Lagally, *Phys. Rev. Lett.* **65**, 1020 (1990).
- ¹⁶D. Leonard, M. Krishnamurthy, C. M. Reeves, S. P. Denbaars, and P. M. Petroff, *Appl. Phys. Lett.* **63**, 3203 (1993).
- ¹⁷J. M. Moison, F. Houzay, F. Barthe, L. Leprince, E. André, and O. Vatel, *Appl. Phys. Lett.* **64**, 196 (1994).
- ¹⁸M. Grundmann, J. Christen, N. N. Ledentsov, J. Böhrer, D. Bimberg, S. S. Ruvimov, P. Werner, U. Richter, U. Gösele, J. Heydenreich, V. M. Ustinov, A. Y. Egorov, A. E. Zhukov, P. S. Kop'ev, and Z. I. Alferov, *Phys. Rev. Lett.* **74**, 4043 (1995).
- ¹⁹S. H. Brongersma, M. R. Castell, D. D. Perovic, and M. Zinke-Allmann, *Phys. Rev. Lett.* **80**, 3795 (1998).
- ²⁰V. I. Marchenko, *JETP Lett.* **33**, 381 (1981).
- ²¹O. L. Alerhand, D. Vanderbilt, R. D. Meade, and J. D. Joannopoulos, *Phys. Rev. Lett.* **61**, 1973 (1988).
- ²²D. Vanderbilt, O. L. Alerhand, R. D. Meade, and J. D. Joannopoulos, *J. Vac. Sci. Technol. B* **7**, 1013 (1989).
- ²³P. Zeppenfeld, M. Krzyzowski, C. Romainczyk, G. Comsa, and M. G. Lagally, *Phys. Rev. Lett.* **72**, 2737 (1994).
- ²⁴Adam Li, Feng Liu, and M. G. Lagally, *Phys. Rev. Lett.* **85**, 1922 (2000).
- ²⁵M. T. Middel, H. J. W. Zandvliet, and B. Poelsema, *Phys. Rev. Lett.* **88**, 196105 (2002).
- ²⁶J. Tersoff and R. M. Tromp, *Phys. Rev. Lett.* **70**, 2782 (1993).
- ²⁷K. D. Develos, H. Yamasaki, A. Sawa, and Y. Nakagawa, *Physica C* **361**, 121 (2001).
- ²⁸Recently, we measured precisely the *ex situ* annealing temperature and found that the actual annealing temperature in Ref. 13 should be 1025 °C instead of 1000 °C.
- ²⁹K. Omote, *X-Ray Spectrom.* **28**, 440 (1999).
- ³⁰M. Ofuji, K. Inaba, K. Omote, H. Hoshi, Y. Takanishi, K. Ishikawa, H. Takezoe, *Jpn. J. Appl. Phys., Part 1* **41**, 5467 (2002).
- ³¹The thickness of CeO_2 films was determined by the XRD Laue oscillations using $t = \lambda / 2[\sin(\theta_i) - \sin(\theta_{i-1})]$, where θ_i and θ_{i-1} are the positions of adjacent satellites.
- ³²T. X. T. Sayle, S. C. Parker, and C. R. A. Catlow, *Surf. Sci.* **316**, 329 (1994).
- ³³J. C. Conesa, *Surf. Sci.* **339**, 337 (1995).
- ³⁴See, e.g., J. C. Bean, *Science* **230**, 127 (1985).
- ³⁵Morphology shown in Figs. 1(b), 1(d), 1(f), and 1(h) and Fig. 2 was not achieved by changing the deposition conditions, e.g., by increasing the deposition temperature up to 840 °C (the upper limit of our apparatus), by changing the laser energy and thus the deposition rate, or by *in situ* O_2 annealing. No matter how to vary the deposition conditions within our apparatus limits, the

- as-grown films (without the *ex situ* high-temperature O₂ annealing) always showed similar morphologies composed of small, round-shaped, and coalesced islands, such as Figs. 1(a), 1(c), 1(e), and 1(g).
- ³⁶V. A. Shchukin, N. N. Ledentsov, P. S. Kop'ev, and D. Bimberg, *Phys. Rev. Lett.* **75**, 2968 (1995).
- ³⁷V. A. Shchukin, A. I. Borovkov, N. N. Ledentsov, and D. Bimberg, *Phys. Rev. B* **51**, 10 104 (1995).
- ³⁸David Vanderbilt and L. K. Wickham, in *Evolution of Thin-Film and Surface Microstructure*, edited by C. V. Thompson, J. Y. Tsao, and D. J. Srolovitz, *Mater. Res. Soc. Symp. Proc.* Vol. 202 (Materials Research Society, Pittsburgh, 1991), p. 555.
- ³⁹B. G. Orr, D. Kessler, and C. W. Snyder, *Europhys. Lett.* **19**, 33 (1992).
- ⁴⁰V. I. Marchenko, *Zh. Eksp. Teor. Fiz.* **81**, 1141 (1981) [*Sov. Phys. JETP* **54**, 605 (1981)].
- ⁴¹S. M. Wiederhorn, *J. Am. Ceram. Soc.* **52**, 485 (1969).
- ⁴²J. B. Hannon, J. Tersoff, and R. M. Tromp, *Science* **295**, 299 (2002).